Letter

Time-dependent ghost Gutzwiller nonequilibrium dynamics

Daniele Guerci [1], Massimo Capone,[2,3] and Nicola Lanatà [4,1,*]

[1] *Center for Computational Quantum Physics, Flatiron Institute, New York, New York 10010, USA*

[2] *Scuola Internazionale Superiore di Studi Avanzati (SISSA), Via Bonomea 265, 34136 Trieste, Italy*

[3] *CNR-IOM, Istituto Officina dei Materiali, Consiglio Nazionale delle Ricerche, Via Bonomea 265, 34136 Trieste, Italy*

[4] *School of Physics and Astronomy, Rochester Institute of Technology, 84 Lomb Memorial Drive, Rochester, New York 14623, USA*

(Received 24 March 2023; revised 29 June 2023; accepted 10 July 2023; published 17 August 2023)

We introduce the time-dependent ghost Gutzwiller approximation (TD-gGA), a nonequilibrium extension of the ghost Gutzwiller approximation (gGA), a powerful variational approach which systematically improves on the standard Gutzwiller method by including auxiliary degrees of freedom. We demonstrate the effectiveness of TD-gGA by studying the quench dynamics of the single-band Hubbard model as a function of the number of auxiliary parameters. Our results show that TD-gGA captures the relaxation of local observables, in contrast with the time-dependent Gutzwiller method. This systematic and qualitative improvement leads to an accuracy comparable with time-dependent dynamical mean-field theory which comes at a much lower computational cost. These findings suggest that TD-gGA has the potential to enable extensive and accurate theoretical investigations of multiorbital correlated electron systems in nonequilibrium situations, with potential applications in the field of quantum control, Mott solar cells, and other areas where an accurate account of the nonequilibrium properties of strongly interacting quantum systems is required.

DOI: 10.1103/PhysRevResearch.5.L032023

Introduction. The study of the nonequilibrium dynamics of correlated electron systems has gained significant attention in recent years, ranging from fundamental questions [1] to topics triggered by the emergence of experimental techniques that allow for the investigation of these systems under a variety of conditions. Examples include ultrafast spectroscopy techniques, which allow for the investigation of the dynamics of solid state materials on the femtosecond timescale [2–4], and the use of ultracold atoms in optical lattices [5–13], which allows for the study of correlated quantum systems in a controlled and tunable environment. The development of efficient photovoltaic technologies such as Mott solar cells [14–18], which exploit the peculiar properties of correlated electron systems, is another example of the many directions calling for theoretical tools and frameworks able to investigate quantum many-body systems out of equilibrium.

The paradigmatic model in the study of correlated electron systems is the (single-orbital) Hubbard model, which describes fermionic particles on a lattice experiencing the effects of local repulsive interactions. A huge body of work has focused on the equilibrium properties of this model, while the investigation of the nonequilibrium physics is severely limited by technical aspects. Current state-of-the-art methods, such time-dependent dynamical mean-field theory (TD-DMFT) [19–22], can be indeed computationally demanding for many applications and they are typically limited to relatively short timescales. This situation calls for the development of computationally lighter, yet sufficiently accurate, methods to study the dynamics of the Hubbard model and possibly of more involved and richer models.

To address this challenge, here we exploit the so-called ghost Gutzwiller approximation (gGA) [23–25], that generalizes the standard Gutzwiller approximation (GA) [26,27] systematically extending the variational space introducing auxiliary degrees of freedom. This perspective introduces similarities between this variational wave function and matrix-product states or more recent neural network states [28] where the number of "hidden" degrees of freedom is directly connected with the amount of entanglement in the variational wave function. Recently, the method has been formulated also in terms of a formally exact rotationally invariant slave boson theory (RISB) [29–32], that reduces to the gGA within the mean-field approximation. In equilibrium, the addition of $\mathcal{B}$ subsidiary fermionic degrees of freedom improves consistently the accuracy of the wave function, and allows for a faithful description of the Mott insulator which reproduces the main results of DMFT already for small values of $\mathcal{B} \lesssim 7$ [33–35].

In this Letter, we introduce a nonequilibrium extension of the gGA framework, that generalizes the standard time-dependent Gutzwiller approximation [36–46]. We apply the method to an interaction quench in the half-filled Hubbard model, a topic which attracted considerable interest, both in experiments [47–49] and theoretical investigations [19–22,50,51].

We show that the improvement introduced by TD-gGA is substantial and qualitative. In particular, this method captures the relaxation of local observables, a crucial feature which

*Corresponding author: nxlsps@rit.edu

is not accessible by the standard time-dependent Gutzwiller approximation [36].

In addition, we show that, using a small number of auxiliary variables, the TD-gGA reproduces the dynamics obtained within TD-DMFT for reasonably large timescales with a significantly reduced computational cost. As we shall describe in the following, the TD-gGA requires indeed to solve a set of nonlinear differential equations as opposed to the integrodifferential equations obtained within TD-DMFT.

Our results highlight the potential of TD-gGA to substantially reduce the computational cost of accurate studies of the time-resolved dynamics of strongly correlated systems. This opportunity can open the path to effective investigations of multiorbital correlated electron systems in nonequilibrium situations, extending the scope to a number of different correlated materials and enabling a variety of applications ranging from energy-related materials [14–18] to quantum control [52], and other areas where the accurate treatment of strong correlations is required.

The plan of this Letter is as follows. First, we introduce the model and we formulate the time-dependent ghost-Gutzwiller approach, and then we apply the tools to study the dynamics of the single-band Hubbard model. The comparison with DMFT results that we thus obtain is discussed after, followed by concluding remarks.

Model and method. We consider the time-dependent dynamics of the single-band Hubbard model at half filling,

$$\hat{H} = \frac{U}{2}\sum_i (\hat{n}_i - 1)^2 - J\sum_{\langle i,j\rangle}\sum_{\sigma=\uparrow,\downarrow}(c^\dagger_{i\sigma}c_{j\sigma} + \text{H.c.}), \quad (1)$$

where U is the Hubbard on-site interaction strength, $\hat{n}_i = \sum_{\sigma=\uparrow,\downarrow} c^\dagger_{i\sigma}c_{i\sigma}$ is the local occupancy operator, and J the hopping between nearest-neighbor sites. We consider the model on a Bethe lattice with a semicircular density of states $\rho(\omega) = 2\sqrt{D^2-\epsilon^2}/(\pi D^2)$ and we measure energy in the unit of the half-bandwidth $D \propto J$. From now on we set D as the energy unit and D^{-1} as the time unit.

In this Letter, we focus on the time-resolved evolution of the system in a popular nonequilibrium protocol, the interaction quench, where the interaction is suddenly changed from U_i to U_f. As a matter of fact, we will evaluate the time evolution governed by Eq. (1) for $U = U_f$ using as an initial state the equilibrium solution for $U = U_i$.

Equilibrium gGA Lagrange function. Specializing the formalism of Refs. [23,24] to the single-orbital model Eq. (1) and enforcing spin rotational invariance and translational invariance, we obtain that the gGA ground state is encoded in the following Lagrange function,

$$\begin{aligned}\mathcal{L}[\Phi, E^c; \mathcal{R}, \Lambda; \mathcal{D}, \Lambda^c; \Delta, \Psi_0, E] &= \frac{1}{\mathcal{N}}\langle\Psi_0|\hat{H}_{\rm qp}[\mathcal{R},\Lambda]|\Psi_0\rangle + E(1-\langle\Psi_0|\Psi_0\rangle)\\ &+ [\langle\Phi|\hat{H}_{\rm emb}[\mathcal{D},\Lambda^c]|\Phi\rangle + E^c(1-\langle\Phi|\Phi\rangle)]\\ &- \Bigg[\sum_{\sigma=\uparrow,\downarrow}\sum_{a,b=1}^{\mathcal{B}}\left(\Lambda_{ab}+\Lambda^c_{ab}\right)\Delta_{ab}\\ &+ \sum_{\sigma=\uparrow,\downarrow}\sum_{c,a=1}^{\mathcal{B}}(\mathcal{D}_a\mathcal{R}_c[\Delta(1-\Delta)]^{\frac{1}{2}}_{ca} + \text{c.c.})\Bigg], \quad (2)\end{aligned}$$

where $\mathcal{N}$ is the total number of unit cells, E and E^c are real numbers, Δ, Λ^c, and Λ are $\mathcal{B}\times\mathcal{B}$ Hermitian matrices, and $\mathcal{D}$ and $\mathcal{R}$ are rectangular $\mathcal{B}\times 1$ matrices (whose row entries are $\mathcal{D}_a$ and $\mathcal{R}_a$, respectively). The auxiliary Hamiltonians $\hat{H}_{\rm qp}$ and $\hat{H}_{\rm emb}$, which are called the "quasiparticle Hamiltonian" and "embedding Hamiltonian" (EH), respectively, are defined as follows:

$$\begin{aligned}\hat{H}_{\rm qp} &= -J\sum_{\langle i,j\rangle}\sum_{a,b=1}^{\mathcal{B}}\sum_{\sigma=\uparrow,\downarrow}\mathcal{R}_a\mathcal{R}^\dagger_b f^\dagger_{ia\sigma}f_{jb\sigma}\\ &+ \sum_i\sum_{a,b=1}^{\mathcal{B}}\sum_{\sigma=\uparrow,\downarrow}\Lambda_{ab}f^\dagger_{ia\sigma}f_{ib\sigma}\\ &= \sum_{a,b=1}^{\mathcal{B}}\sum_{\omega=1}^{\mathcal{N}}\sum_{\sigma=\uparrow,\downarrow}(\epsilon_\omega\,\mathcal{R}_a\mathcal{R}^\dagger_b + \Lambda_{ab})\eta^\dagger_{\omega a\sigma}\eta_{\omega b\sigma}, \quad (3)\\ \hat{H}_{\rm emb} &= \frac{U}{2}(\hat{n}-1)^2 + \sum_{a=1}^{\mathcal{B}}\sum_{\sigma=\uparrow,\downarrow}[\mathcal{D}_a\,\hat{c}^\dagger_\sigma\hat{f}_{a\sigma} + \text{H.c.}]\\ &+ \sum_{a,b=1}^{\mathcal{B}}\sum_{\sigma=\uparrow,\downarrow}\Lambda^c_{ab}\hat{f}_{b\sigma}\hat{f}^\dagger_{a\sigma}, \quad (4)\end{aligned}$$

where ϵ_ω are the eigenvalues of the hopping matrix for the Bethe lattice, $\eta_{\omega\sigma}$ are the corresponding eigenmodes, and $\hat{n} = \sum_{\sigma=\uparrow,\downarrow}\hat{c}^\dagger_\sigma\hat{c}_\sigma$ is the impurity occupancy operator.

The integer parameter $\mathcal{B}$ controls the size of the variational space and, in turn, the accuracy of the gGA solution. In particular, for $\mathcal{B} = 1$, Eq. (2) reduces to the standard GA Lagrange function, while for higher values of $\mathcal{B}$ the accuracy of the gGA method is comparable to DMFT [23,24].

The saddle point of the Lagrangian $\mathcal{L}$ defined in Eq. (2) is given by the following equations,

$$\int_{-D}^{D} d\omega\,\rho(\omega)[n(\omega)]_{ab} = \Delta_{ab}, \quad (5)$$

$$\int_{-D}^{D} d\omega\,\rho(\omega)\omega[\mathcal{R}^{\dagger\,t}n(\omega)]_{1a} = \sum_{c,a=1}^{\mathcal{B}}\mathcal{D}_c[\Delta(1-\Delta)]^{\frac{1}{2}}_{ac}, \quad (6)$$

$$\sum_{c,b=1}^{\mathcal{B}}\frac{\partial}{\partial d_s}([\Delta(1-\Delta)]^{\frac{1}{2}}_{cb}\mathcal{D}_b\mathcal{R}_c + \text{c.c.}) + [l+l^c]_s = 0, \quad (7)$$

$$\hat{H}^{\rm emb}|\Phi\rangle = E^c|\Phi\rangle, \quad (8)$$

$$\mathcal{F}^{(1)}_a = \langle\Phi|\hat{c}^\dagger_\sigma\hat{f}_{a\sigma}|\Phi\rangle - \sum_{c=1}^{\mathcal{B}}[\Delta(1-\Delta)]^{\frac{1}{2}}_{ca}\mathcal{R}_c = 0, \quad (9)$$

$$\mathcal{F}^{(2)}_{ab} = \langle\Phi|\hat{f}_{b\sigma}\hat{f}^\dagger_{a\sigma}|\Phi\rangle - \Delta_{ab} = 0, \quad (10)$$

where Eqs. (5) and (6) are evaluated for the Bethe lattice at $\mathcal{N}\to\infty$ and the limit of infinite coordination number, ${}^tM$ indicates the transpose of a matrix M,

$$[n(\omega)]_{ab} = \langle\Psi_0|\eta^\dagger_{\omega a\sigma}\eta_{\omega b\sigma}|\Psi_0\rangle = [f\left(\mathcal{R}\omega\mathcal{R}^\dagger + \Lambda\right)]_{ba} \quad (11)$$

is the quasiparticle ground-state single-particle density matrix in the Bethe lattice eigenmodes basis, f is the zero-temperature Fermi function, and we expressed the matrices Δ, Λ, and Λ^c in terms of the following expansion with respect to

an orthonormal basis of Hermitian matrices $\{h_s\}$ (with respect to the canonical scalar product $(A, B) = \mathrm{Tr}[A^\dagger B]$),

$$\Delta = \sum_{s=1}^{\mathcal{B}^2} d_s{}^t h_s, \tag{12}$$

$$\Lambda = \sum_{s=1}^{\mathcal{B}^2} l_s\, h_s, \tag{13}$$

$$\Lambda^c = \sum_{s=1}^{\mathcal{B}^2} l_s^c\, h_s, \tag{14}$$

where d_s, l_s, and l_s^c are real-valued coefficients.

Algorithmic structure of the gGA. Equations (5)–(10) can be solved numerically as follows: (1) Starting from an initial guess for the entries $\mathcal{R}$ and Λ, compute Δ from Eq. (5). (2) Compute $\mathcal{D}$ using Eq. (6). (3) Determine the coefficients l_s^c from Eq. (7) and construct the matrix Λ^c from Eq. (14). (4) Construct $\hat{H}^{\mathrm{emb}}$ from Eq. (4) and calculate its ground state $|\Phi\rangle$ within the subspace with $1+\mathcal{B}$ fermions (i.e., at half filling). (5) Compute $\mathcal{F}^{(1)}$ and $\mathcal{F}^{(2)}$ from Eqs. (9) and (10). The parameters $(\mathcal{R}, \Lambda)$ such that Eqs. (9) and (10) are satisfied are computed numerically.

Time-dependent gGA Lagrange function. As explained in Refs. [23,24], the equilibrium gGA Lagrange function and equations summarized above can be obtained by applying the standard standard multiorbital GA formulation of Ref. [27] within an enlarged Hilbert space, including additional auxiliary fermionic degrees of freedom. Equivalently, the same equations can be derived from the standard multiorbital formulation of Ref. [30], by introducing additional auxiliary fermionic and bosonic degrees of freedom [29]. The TD-gGA framework is straightforwardly obtained by applying the standard TD-GA formalism of Ref. [36], simply by including such auxiliary degrees of freedom mentioned above, either from the GA perspective [53] or, equivalently, from the RISB [29] perspective. The resulting dynamics is obtained by extremizing the following Lagrange function, previously introduced in Ref. [29],

$$\begin{aligned}\mathcal{L} = {} & \frac{1}{\mathcal{N}}\langle\Psi_0|i\partial_t - \hat{H}_{\mathrm{qp}}|\Psi_0\rangle + \langle\Phi|i\partial_t - \hat{H}_{\mathrm{emb}}|\Phi\rangle \\ & + \Bigg[\sum_{\sigma=\uparrow,\downarrow}\sum_{a,b=1}^{\mathcal{B}} \Lambda^c_{ab}\Delta_{ab} \\ & + \sum_{\sigma=\uparrow,\downarrow}\sum_{c,a=1}^{\mathcal{B}} \left(\mathcal{D}_a\mathcal{R}_c[\Delta(1-\Delta)]^{\frac{1}{2}}_{ca} + \mathrm{c.c.}\right)\Bigg],\end{aligned} \tag{15}$$

where $\hat{H}_{\mathrm{qp}}$ and $\hat{H}_{\mathrm{emb}}$ are given by Eqs. (3) and (4), respectively, setting $\Lambda = 0$.

As for the equilibrium case, the stationarity conditions with respect to Δ, $\mathcal{D}$, and Λ^c are Eqs. (7), (9), and (10), respectively. Instead, from the Dirac-Frenkel principle it follows that the stationarity conditions with respect to $|\Psi_0\rangle$ and $|\Phi\rangle$ are the corresponding time-dependent Schrödinger equations. In summary, the dynamics of the gGA variational parameters is governed by the following equations,

$$[i\partial_t - \hat{H}_{\mathrm{emb}}]|\Phi\rangle = 0, \tag{16}$$

$$i\partial_t n_{ab}(\omega) = \omega\sum_{c=1}^{\mathcal{B}}[\mathcal{R}_b\mathcal{R}_c^\dagger n_{ac}(\omega) - \mathcal{R}_c\mathcal{R}_a^\dagger n_{cb}(\omega)], \tag{17}$$

$$\int_{-D}^{D} d\omega\,\rho(\omega)\,\omega[\mathcal{R}^\dagger{}^t n(\omega)]_{1a} = \sum_{c,a=1}^{\mathcal{B}} \mathcal{D}_c[\Delta(1-\Delta)]^{\frac{1}{2}}_{ac}, \tag{18}$$

$$\sum_{c,b=1}^{\mathcal{B}} \frac{\partial}{\partial d_s}([\Delta(1-\Delta)]^{\frac{1}{2}}_{cb}\mathcal{D}_b\mathcal{R}_c + \mathrm{c.c.}) + l_s^c = 0, \tag{19}$$

$$\langle\Phi|\hat{c}_\sigma^\dagger\hat{f}_{a\sigma}|\Phi\rangle - \sum_{c=1}^{\mathcal{B}}[\Delta(1-\Delta)]^{\frac{1}{2}}_{ca}\mathcal{R}_c = 0, \tag{20}$$

$$\langle\Phi|\hat{f}_{b\sigma}\hat{f}_{a\sigma}^\dagger|\Phi\rangle - \Delta_{ab} = 0, \tag{21}$$

where Eq. (17) describes the time evolution of the quasiparticle single-particle density matrix corresponding to the following time-dependent Schrödinger equation $[i\partial_t - \hat{H}_{\mathrm{qp}}]|\Psi_0\rangle = 0$.

To implement the dynamics governed by Eqs. (16)–(21) the integrals over ω are approximated by discretizing the interval $[-D, D]$ with a series of frequencies ω_n. The real and imaginary components of the vector Φ and of the matrices $n(\omega_n)$ are encoded into a real-valued vector $\mathbf{Y}$. Since $\mathcal{R}$, $\mathcal{D}$, Δ, and Λ^c can be all determined as a function of $|\Phi\rangle$ and $n(\omega)$ using Eqs. (19)–(21), and $\partial_t|\Phi\rangle$ and $\partial_t n(\omega)$ can be determined in terms of these parameters using Eqs. (16) and (17), the dynamics of $\mathbf{Y}$ can be expressed as follows,

$$\partial_t\mathbf{Y}(t) = \mathbf{F}(\mathbf{Y}(t)), \tag{22}$$

which is a nonlinear first-order differential equation that can be integrated numerically with standard methods. In particular, our calculations were performed using the the Runge-Kutta library RKSUITE [54].

It is important to note that the function $\mathbf{F}$ used in our study of Hubbard quenches is independent of time when the Hamiltonian is not explicitly time dependent after the sudden change in U. However, the equations we derived can still be used even if the Hamiltonian has an explicit time dependence. In this case, the TD-gGA equations take the form

$$\partial_t\mathbf{Y}(t) = \mathbf{F}(\mathbf{Y}(t), \mathbf{A}(t)), \tag{23}$$

where $\mathbf{A}(t)$ represents a time-varying external perturbation, such as an electromagnetic field. This characteristic of the TD-gGA framework is particularly interesting, because it opens the possibility of using standard frameworks, such as classical optimal control algorithms [52], for manipulating the dynamics of electronic states. In fact, such techniques are broadly applicable to dynamical systems governed by ordinary differential equations such as Eq. (23), while frameworks for controlling the TD-DMFT dynamics, governed by integrodifferential equations, are not currently available.

Interaction quench in the half-filled Hubbard model. We now turn to the application of the formalism to discuss the out-of-equilibrium evolution in the half-filled single-band Hubbard model (1). The quantum quench protocol consists of preparing the system in the initial variational ground state of

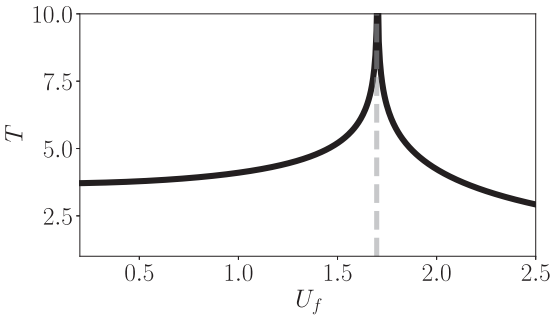

FIG. 1. Period of the coherent oscillations in the dynamics of the single-band Hubbard model in the conventional Gutwiller approximation ($\mathcal{B} = 1$) as a function of U_f. The divergence at $U_c^{\rm dyn} = U_c/2$ defined by the dashed gray vertical line shows the critical slowing down at the dynamical transition [37,56].

the model with interaction $U(t \leqslant 0) = U_i$. Then, for $t > 0$, the state evolves under an Hamiltonian characterized by the value of the interaction $U(t > 0) = U_f = U_i + \delta U \neq U_i$.

We focus our analysis by considering as initial condition a weakly correlated metal $U_i \simeq 0$ and the final interaction strength is larger than the initial value $U_f > U_i$ [55]. Under these circumstances, the standard TD-GA dynamics (corresponding to $\mathcal{B} = 1$ in our formalism) is characterized by the presence of a dynamical quantum critical point that identifies three different dynamical regimes of weak $U_f < U_c^{\rm dyn}$, intermediate $U_f \sim U_c^{\rm dyn}$, and strong $U_f > U_c^{\rm dyn}$ quenches [37]. Within this framework ($\mathcal{B} = 1$) different regimes were identified by computing the period of oscillation of the time-dependent double occupancy $d(t) = \langle \Phi(t)|n_\uparrow n_\downarrow|\Phi(t)\rangle$ following the quench, which is purely monochromatic (see Fig. 1).

Below we show the TD-gGA time evolution of the double occupancy $d(t)$ as a function of $\mathcal{B}$, in comparison with the numerically exact TD-DMFT results of Ref. [20], for different values of U_f, spanning all the different dynamical regimes [see Fig. 2(a)]. In order to better interpret the results we also show the time evolution of the eigenvalues of Λ^c and $\sqrt{\mathcal{D}^\dagger\mathcal{D}}$, which are both gauge-invariant quantities associated with the dynamics of the EH [see Fig. 2(b)]. Specifically, the eigenvalues of the matrix Λ^c are the energies of the bath in the EH [see Eq. (4)]. The quantity $\sqrt{\mathcal{D}^\dagger\mathcal{D}}$ is the sum of the absolute square values of the tunneling couplings $\mathcal{D}_a$ between the impurity

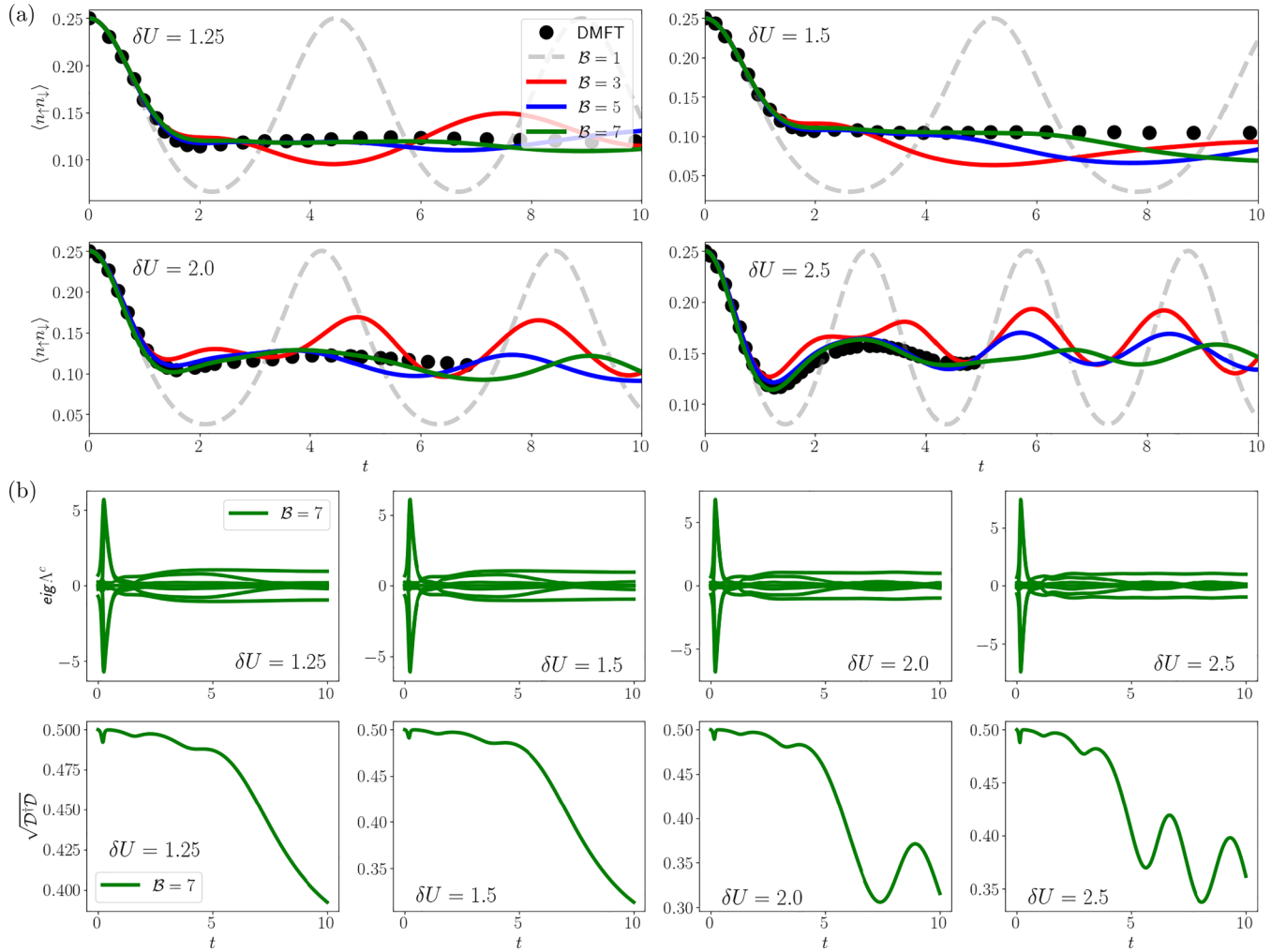

FIG. 2. (a) Evolution of the double occupancies as a function of time for different values of δU, in sequence $\delta U = 1.25, 1.5, 2.0, 2.5$, respectively. The dotted data show the DMFT result taken from Ref. [20]. Different colors correspond to different values of $\mathcal{B}$ (number of bath sites). (b) The top row shows the evolution of the eigenvalues of the Λ^c for $\mathcal{B} = 7$. The bottom row displays the evolution of $\sqrt{\mathcal{D}^\dagger\mathcal{D}}$ for $\mathcal{B} = 7$.

and its environment, acting as a measure of the hybridization strength between them as a function of time. Note that plotting the evolution of eig Λ^c and $\sqrt{\mathcal{D}^\dagger \mathcal{D}}$ allows us to detect the physical dynamics of the embedding parameters, decoupling it from irrelevant time-dependent gauge transformations.

Our results show that, while within the standard TD-GA ($\mathcal{B} = 1$) the evolution of $d(t)$ is accurate only at very short times and does not capture the relaxation of the double occupancy at long times which is observed in TD-DMFT, for $\mathcal{B} \geqslant 3$ we develop a clear trend towards a relaxation of the local observables which replaces the oscillations obtained for $\mathcal{B} = 1$. The improvement introduced by introducing the auxiliary degrees of freedom approaches the TD-DMFT dynamics with increasingly high accuracy. Indeed, the TD-gGA dynamics follows the DMFT reference on a timescale that increases as we increase $\mathcal{B}$. For instance, we note that for values as small as $\mathcal{B} = 7$ the method achieves nearly perfect agreement with TD-DMFT for $t \lesssim 6$, for all quenches considered. The recurrence of oscillations after a characteristic timescale at finite $\mathcal{B}$ can be interpreted as a "finite-size" effect of the EH bath. Following this argument, we expect that in the TD-gGA dynamics local observables will eventually approach the steady state as $\mathcal{B}$ tends to infinity. We leave a detailed exploration of the time evolution in the limit of large $\mathcal{B}$ to future studies. It is interesting to note that the TD-gGA dynamics of the double occupancy arises from the time-dependent Schrödinger equation [Eq. (16)], and the parameters of the corresponding EH shown in the middle and right columns of the figure evolve in time even when $d(t)$ appears to be essentially stationary. This is consistent with the general fact that the equilibration arises for local quantities, such as the double occupancy, even though the quantum dynamics of the many-body electronic function, here encoded in the time evolution of the TD-gGA variational parameters, is unitary.

Conclusions. In this Letter, we introduced a time-dependent extension of the ghost Gutzwiller approximation (gGA) for the study of correlated electron systems in nonequilibrium situations. We have benchmarked the method for an interaction quench of the half-filled Hubbard model, comparing explicitly with one of the state-of-the-art approaches, TD-DMFT.

Our results clearly show that this approach, already for a small number $\mathcal{B}$ of auxiliary parameters, improves qualitatively on the standard Gutzwiller approximation, since it can describe the relaxation of local observables, and it achieves a remarkable quantitative agreement with TD-DMFT for a wide range of model parameters and timescales already for small values of $\mathcal{B}$.

A crucial point is that an accuracy comparable with TD-DMFT is thus obtained at a hugely smaller computational cost since the TD-gGA requires to solve a nonlinear ordinary differential equation as opposed to the integro-differential equation required by TD-DMFT. The computational burden of each TD-gGA time step [as per Eqs. (16)–(21)] is considerably lower than that of each static gGA iteration [as per Eqs. (5)–(10)]. The primary reason is that the key source of computational complexity in each TD-gGA time step—the matrix-vector multiplication in Eq. (16)—is less taxing than the embedding-Hamiltonian eigenvalue problem of Eq. (8), which is the main computational demand in the static gGA. As a result, the overall cost of a TD-gGA computation is largely determined by the number of time steps and the tightness of the mesh used by the adaptive Runge-Kutta method, which depend on the desired numerical accuracy and the specific dynamics of the system under study. Importantly, these operations are, in principle, parallelizable, which leads to additional computational cost reductions.

In particular, all calculations performed in this Letter have been performed serially on a single CPU, highlighting the method's computational efficiency. Utilizing methods such as time-dependent density matrix renormalization group (DMRG) [57,58] or matrix products states (MPS) [59–62] to solve the time-dependent Schrödinger equation of the EH would allow us to reduce the computational complexity even further, allowing us to perform calculations with more bath sites, even for multiorbital strongly correlated systems. Furthermore, the very fact that TD-gGA ultimately reduces to a finite-dimensional first-order nonlinear differential equation, allows one to employ, e.g., optimal control methods to steer a given dynamical system to desired outcomes. These observations suggest that the TD-gGA has the potential to advance our ability to study the nonequilibrium properties of a variety of systems of great interest, ranging from the general study of multiorbital correlated electron materials to quantum devices including Mott solar cells [14–18], or more in general to any problem which requires a proper treatment of electronic correlations while accessing nonequilibrium properties.

Acknowledgments. We are indebted to Michele Fabrizio for his insightful contributions at the early stage of the project. We also acknowledge discussions with Marco Schiró, Carlos Mejuto Zaera, and Jan Skolimowski. The Flatiron Institute is a division of the Simons Foundation. This work was supported by a grant from the Simons Foundation (1030691, NL). M.C. acknowledges financial support from MUR via PNRR MUR Project No. PE0000023-NQSTI, PNNR National Center for HPC, Big Data, and Quantum Computing (Grant No. CN00000013), PRIN 2020 q-LIMA (Protocol No. 2020JLZ52N), and PRIN 2017 CEnTral (Protocol No. 20172H2SC4).

[1] A. Polkovnikov, K. Sengupta, A. Silva, and M. Vengalattore, Colloquium: Nonequilibrium dynamics of closed interacting quantum systems, Rev. Mod. Phys. **83**, 863 (2011).

[2] A. Cavalleri, C. Tóth, C. W. Siders, J. A. Squier, F. Ráksi, P. Forget, and J. C. Kieffer, Femtosecond Structural Dynamics in VO_2 During an Ultrafast Solid-Solid Phase Transition, Phys. Rev. Lett. **87**, 237401 (2001).

[3] C. Giannetti, M. Capone, D. Fausti, M. Fabrizio, F. Parmigiani, and D. Mihailovic, Ultrafast optical spectroscopy of strongly correlated materials and high-temperature superconductors: a non-equilibrium approach, Adv. Phys. **65**, 58 (2016).

[4] A. de la Torre, D. M. Kennes, M. Claassen, S. Gerber, J. W. McIver, and M. A. Sentef, Colloquium: Nonthermal pathways to ultrafast control in quantum materials, Rev. Mod. Phys. **93**, 041002 (2021).

[5] D. Jaksch, V. Venturi, J. I. Cirac, C. J. Williams, and P. Zoller, Creation of a Molecular Condensate by Dynamically Melting a Mott Insulator, Phys. Rev. Lett. **89**, 040402 (2002).

[6] D. Jaksch and P. Zoller, The cold atom Hubbard toolbox, Ann. Phys. **315**, 52 (2005).

[7] I. Bloch, J. Dalibard, and W. Zwerger, Many-body physics with ultracold gases, Rev. Mod. Phys. **80**, 885 (2008).

[8] T. Esslinger, Fermi-Hubbard physics with atoms in an optical lattice, Annu. Rev. Condens. Matter Phys. **1**, 129 (2010).

[9] I. Bloch, J. Dalibard, and S. Nascimbène, Quantum simulations with ultracold quantum gases, Nat. Phys. **8**, 267 (2012).

[10] A. Mazurenko, C. S. Chiu, G. Ji, M. F. Parsons, M. Kanász-Nagy, R. Schmidt, F. Grusdt, E. Demler, D. Greif, and M. Greiner, A cold-atom Fermi–Hubbard antiferromagnet, Nature (London) **545**, 462 (2017).

[11] J. H. Drewes, L. A. Miller, E. Cocchi, C. F. Chan, N. Wurz, M. Gall, D. Pertot, F. Brennecke, and M. Köhl, Antiferromagnetic Correlations in Two-Dimensional Fermionic Mott-Insulating and Metallic Phases, Phys. Rev. Lett. **118**, 170401 (2017).

[12] M. Yan, H.-Y. Hui, M. Rigol, and V. W. Scarola, Equilibration Dynamics of Strongly Interacting Bosons in 2D Lattices with Disorder, Phys. Rev. Lett. **119**, 073002 (2017).

[13] M. Yan, H.-Y. Hui, and V. W. Scarola, Dynamics of disordered states in the Bose-Hubbard model with confinement, Phys. Rev. A **95**, 053624 (2017).

[14] E. Manousakis, Photovoltaic effect for narrow-gap Mott insulators, Phys. Rev. B **82**, 125109 (2010).

[15] P. Werner, K. Held, and M. Eckstein, Role of impact ionization in the thermalization of photoexcited Mott insulators, Phys. Rev. B **90**, 235102 (2014).

[16] L. Wang, Y. Li, A. Bera, C. Ma, F. Jin, K. Yuan, W. Yin, A. David, W. Chen, W. Wu, W. Prellier, S. Wei, and T. Wu, Device Performance of the Mott Insulator $LaVO_3$ as a Photovoltaic Material, Phys. Rev. Appl. **3**, 064015 (2015).

[17] F. Petocchi, S. Beck, C. Ederer, and P. Werner, Hund excitations and the efficiency of Mott solar cells, Phys. Rev. B **100**, 075147 (2019).

[18] F. Petocchi, J. Chen, J. Li, M. Eckstein, and P. Werner, Photoinduced charge dynamics in $1T$-TaS_2, Phys. Rev. B **107**, 165102 (2023).

[19] H. Aoki, N. Tsuji, M. Eckstein, M. Kollar, T. Oka, and P. Werner, Nonequilibrium dynamical mean-field theory and its applications, Rev. Mod. Phys. **86**, 779 (2014).

[20] M. Eckstein, M. Kollar, and P. Werner, Thermalization after an Interaction Quench in the Hubbard Model, Phys. Rev. Lett. **103**, 056403 (2009).

[21] M. Eckstein, M. Kollar, and P. Werner, Interaction quench in the Hubbard model: Relaxation of the spectral function and the optical conductivity, Phys. Rev. B **81**, 115131 (2010).

[22] A. Georges, G. Kotliar, W. Krauth, and M. J. Rozenberg, Dynamical mean-field theory of strongly correlated fermion systems and the limit of infinite dimensions, Rev. Mod. Phys. **68**, 13 (1996).

[23] N. Lanatà, T.-H. Lee, Y.-X. Yao, and V. Dobrosavljević, Emergent Bloch excitations in Mott matter, Phys. Rev. B **96**, 195126 (2017).

[24] M. S. Frank, T.-H. Lee, G. Bhattacharyya, P. K. H. Tsang, V. L. Quito, V. Dobrosavljević, O. Christiansen, and N. Lanatà, Quantum embedding description of the anderson lattice model with the ghost Gutzwiller approximation, Phys. Rev. B **104**, L081103 (2021).

[25] D. Guerci, M. Capone, and M. Fabrizio, Exciton Mott transition revisited, Phys. Rev. Mater. **3**, 054605 (2019).

[26] M. C. Gutzwiller, Correlation of electrons in a narrow *s* band, Phys. Rev. **137**, A1726 (1965).

[27] N. Lanatà, Y. Yao, C.-Z. Wang, K.-M. Ho, and G. Kotliar, Phase Diagram and Electronic Structure of Praseodymium and Plutonium, Phys. Rev. X **5**, 011008 (2015).

[28] J. R. Moreno, G. Carleo, A. Georges, and J. Stokes, Fermionic wave functions from neural-network constrained hidden states, Proc. Natl. Acad. Sci. USA **119**, e2122059119 (2022).

[29] N. Lanatà, Operatorial formulation of the ghost rotationally invariant slave-boson theory, Phys. Rev. B **105**, 045111 (2022).

[30] N. Lanatà, Y. Yao, X. Deng, V. Dobrosavljević, and G. Kotliar, Slave Boson Theory of Orbital Differentiation with Crystal Field Effects: Application to UO_2, Phys. Rev. Lett. **118**, 126401 (2017).

[31] G. Kotliar and A. E. Ruckenstein, New Functional Integral Approach to Strongly Correlated Fermi Systems: The Gutzwiller Approximation as a Saddle Point, Phys. Rev. Lett. **57**, 1362 (1986).

[32] F. Lechermann, A. Georges, G. Kotliar, and O. Parcollet, Rotationally invariant slave-boson formalism and momentum dependence of the quasiparticle weight, Phys. Rev. B **76**, 155102 (2007).

[33] T.-H. Lee, N. Lanatà, and G. Kotliar, Accuracy of ghost rotationally invariant slave-boson and dynamical mean field theory as a function of the impurity-model bath size, Phys. Rev. B **107**, L121104 (2023).

[34] C. Mejuto-Zaera and M. Fabrizio, Efficient computational screening of strongly correlated materials: Multiorbital phenomenology within the ghost Gutzwiller approximation, Phys. Rev. B **107**, 235150 (2023).

[35] T.-H. Lee, C. Melnick, R. Adler, N. Lanatà, and G. Kotliar, Accuracy of ghost-rotationally-invariant slave-boson theory for multiorbital Hubbard models and realistic materials, arXiv:2305.11128.

[36] M. Fabrizio, The out-of-equilibrium time-dependent Gutzwiller approximation, in *New Materials for Thermoelectric Applications: Theory and Experiment*, edited by V. Zlatic and A. Hewson, NATO Science for Peace and Security Series B: Physics and Biophysics (Springer, Dordrecht, 2013), pp. 247–273.

[37] M. Schiró and M. Fabrizio, Time-Dependent Mean Field Theory for Quench Dynamics in Correlated Electron Systems, Phys. Rev. Lett. **105**, 076401 (2010).

[38] N. Lanatà and H. U. R. Strand, Time-dependent and steady-state Gutzwiller approach for nonequilibrium transport in nanostructures, Phys. Rev. B **86**, 115310 (2012).

[39] G. Seibold and J. Lorenzana, Time-Dependent Gutzwiller Approximation for the Hubbard Model, Phys. Rev. Lett. **86**, 2605 (2001).

[40] E. v. Oelsen, G. Seibold, and J. Bünemann, Time-Dependent Gutzwiller Theory for Multiband Hubbard Models, Phys. Rev. Lett. **107**, 076402 (2011).

[41] M. Schiró, Nonequilibrium dynamics across an impurity quantum critical point due to quantum quenches, Phys. Rev. B **86**, 161101(R) (2012).

[42] M. Sandri, M. Schiró, and M. Fabrizio, Linear ramps of interaction in the fermionic Hubbard model, Phys. Rev. B **86**, 075122 (2012).

[43] M. Sandri and M. Fabrizio, Nonequilibrium dynamics in the antiferromagnetic Hubbard model, Phys. Rev. B **88**, 165113 (2013).

[44] M. M. Wysokiński and M. Fabrizio, Interplay of charge and spin dynamics after an interaction quench in the Hubbard model, Phys. Rev. B **96**, 201115(R) (2017).

[45] G. Mazza, From sudden quench to adiabatic dynamics in the attractive Hubbard model, Phys. Rev. B **96**, 205110 (2017).

[46] D. Guerci, Transport through a magnetic impurity: A slave-spin approach, Phys. Rev. B **99**, 195409 (2019).

[47] R. Jördens, N. Strohmaier, K. Günter, H. Moritz, and T. Esslinger, A Mott insulator of fermionic atoms in an optical lattice, Nature (London) **455**, 204 (2008).

[48] U. Schneider, L. Hackermüller, J. P. Ronzheimer, S. Will, S. Braun, T. Best, I. Bloch, E. Demler, S. Mandt, D. Rasch *et al.*, Fermionic transport and out-of-equilibrium dynamics in a homogeneous Hubbard model with ultracold atoms, Nat. Phys. **8**, 213 (2012).

[49] F. Schäfer, T. Fukuhara, S. Sugawa, Y. Takasu, and Y. Takahashi, Tools for quantum simulation with ultracold atoms in optical lattices, Nat. Rev. Phys. **2**, 411 (2020).

[50] M. Moeckel and S. Kehrein, Interaction Quench in the Hubbard Model, Phys. Rev. Lett. **100**, 175702 (2008).

[51] F. Goth and F. F. Assaad, Time and spatially resolved quench of the fermionic Hubbard model showing restricted equilibration, Phys. Rev. B **85**, 085129 (2012).

[52] F. K. Wilhelm, S. Kirchhoff, S. Machnes, N. Wittler, and D. Sugny, An introduction into optimal control for quantum technologies, arXiv:2003.10132.

[53] D. Guerci, Beyond simple variational approach for strongly correlated electron systems, Ph.D. thesis, Scuola Internazionale Superiore di Studi Avanzati, 2019, https://hdl.handle.net/20.500.11767/103994.

[54] R. Brankin, I. Gladwell, and L. Shampine, RKSUITE: A suite of explicit Runge-Kutta codes, in *Contributions in Numerical Mathematics* (World Scientific, Singapore, 1993), pp. 41–53.

[55] Our calculations have been performed setting the initial state at a very small interaction strength $U_i = 0.05$. This is because the gGA variational landscape is degenerate in the limiting case $U = 0 \forall \mathcal{B} \geqslant 3$ and, therefore, the self-consistency procedure becomes numerically unstable.

[56] M. Schiró and M. Fabrizio, Quantum quenches in the Hubbard model: Time-dependent mean-field theory and the role of quantum fluctuations, Phys. Rev. B **83**, 165105 (2011).

[57] F. A. Wolf, I. P. McCulloch, and U. Schollwöck, Solving nonequilibrium dynamical mean-field theory using matrix product states, Phys. Rev. B **90**, 235131 (2014).

[58] D. Bauernfeind, X. Cao, E. M. Stoudenmire, and O. Parcollet, Minimally entangled typical thermal state algorithms for finite temperature Matsubara Green functions, Phys. Rev. B **105**, 195107 (2022).

[59] J. Prior, A. W. Chin, S. F. Huelga, and M. B. Plenio, Efficient Simulation of Strong System-Environment Interactions, Phys. Rev. Lett. **105**, 050404 (2010).

[60] L. Kohn and G. E. Santoro, Quenching the anderson impurity model at finite temperature: Entanglement and bath dynamics using matrix product states, arXiv:2107.02807.

[61] J. Thoenniss, M. Sonner, A. Lerose, and D. A. Abanin, Efficient method for quantum impurity problems out of equilibrium, Phys. Rev. B **107**, L201115 (2023).

[62] N. Ng, G. Park, A. J. Millis, G. K.-L. Chan, and D. R. Reichman, Real-time evolution of Anderson impurity models via tensor network influence functionals, Phys. Rev. B **107**, 125103 (2023).